Energy Storage Materials 37 (2021) 40–46

Contents lists available at ScienceDirect

Energy Storage Materials

journal homepage: www.elsevier.com/locate/ensm

Research paper

Rationally design lithiophilic surfaces toward high–energy Lithium metal battery

Zhaohuai Li[a], Qiu He[b,c], Cheng Zhou[a], Yan Li[b,c], Zhenhui Liu[a], Xufeng Hong[a], Xu Xu[a,c,*], Yan Zhao[b,c,*], Liqiang Mai[a,d,*]

[a] State Key Laboratory of Advanced Technology for Materials Synthesis and Processing, Wuhan University of Technology, Wuhan 430070, China
[b] State Key Laboratory of Silicate Materials for Architectures, Wuhan University of Technology, Wuhan 430070, China
[c] International School of Materials Science and Engineering, Wuhan University of Technology, Wuhan 430070, China
[d] Foshan Xianhu Laboratory of the Advanced Energy Science and Technology Guangdong Laboratory, Xianhu Hydrogen Valley, Foshan 528200, China

ARTICLE INFO

Keywords:
Homogeneous Li nucleation
in–situ microscope
Lithium metal battery
Lithiophilicity mechanism
First principles calculations

ABSTRACT

The practical application of lithium (Li) metal anode has been hindered by the fast Li depletion and shallow cycling conditions. Herein, a universal and scalable approach for current collectors combining an enhanced lithiophilic surface and a conductive inner core enables a promising pathway for high–performance Li metal battery (LMB). The interface between anode and electrolyte accelerates Li ions self–concentration and enhances the electrokinetic surface conduction with suppressed Li concentration polarization. With Cu@Cu_3N as an example, a fast Li plating/stripping at 20 mA cm^{-2} for 10,000 cycles and a stable full cell under the near realistic conditions with a high active material loading (19.1 mg cm^{-2}), a low electrolyte/active materials ratio (2.3), and a limited Li resource (10.24 mAh cm^{-2}: equivalent to 50 μm Li foil) are achieved for broadening the commercialization of LMB.

1. Introduction

With regards to the high–energy density storage systems research, lithium (Li) anode has been attracting wide attention due to its highest specific capacity (3860 mAh g^{-1}) and lowest redox potential (−3.040 V *vs* standard hydrogen electrode), and it has been regarded as the "Holy Grail" of Li metal battery (LMB) electrode material. [1–9] However, the growth of Li dendrites is caused by uncontrolled repeated Li plating and stripping, leading to the electrode volume expansion, internal short circuit and other serious safety risks, which greatly hinder the development and commercialization of LMB. [10–14] Extensive efforts in recent years have focused on current collector engineering, which is considered as a promising and pragmatic approach to stabilize Li anode because of its ability of inhibiting the dendrite growth and buffering the unlimited volume expansion of Li. [15–24]

In particular, 3D–structured electrode materials have been attracting great attentions, which feature high specific areas with abundant active sites, enabling the homogenization of Li ion concentration near the electrode surface as well as the acceleration of the uniform Li ion flux deposition and rapid re–distribution even at high current densities. [25–35] Stimulating by the reinforced SEI with lithium nitride (Li_3N), [36,37] copper nitride (Cu_3N) has been successfully applied to the interface and current collector engineering for Li metal dendrite suppression due to its stable chemical structure, high ionic conductivity and excellent affinity to Li. [38–40] However, the elaborate specific structure of conductive framework requires complicated and time–consuming construction process, which is keeping it far from industrial applications. Additionally, growth of metal dendrites is strongly affected by the Li ion concentration near the electrode surface, which is closely related to current density. Most reports in literature ignore that Li metal anode circulates at relatively low capacity (< 5 mAh cm^{-2}) and current density (< 5 mA cm^{-2}), which significantly limits its high energy/power density and causing ineffective Li utilization (< 1%). [12,41]

Herein, we proposed a facile and scalable strategy to construct an ultra–lithiophilic Cu_3N nanoparticles decorated 3D M (M = copper (Cu), zinc (Zn), Cobalt (Co), nickel (Ni), carbon paper (C), et al.) skeletons (M@Cu_3N) for Li integration (Fig. 1, Fig. S1 and S2). The synergistic architecture of Cu@Cu_3N combines an enhanced lithiophilic surface with highly conductive inner core and facilitates uniform and fast Li transportation, reduces the Li nuclear overpotential and extends the lifespan of cells. Because of the superior affinity to Li, the anode/electrolyte interface could accelerate Li ions self–concentration and promote the homogeneous Li transport with suppressed Li ions concentration polarization. [42] Furthermore, the interspaces among the skeletons provide enough space for Li deposition, laying the foundation to achieve higher Li deposition capacity towards high energy density LMB. By realizing

* Corresponding authors.
E-mail addresses: xuxu@whut.edu.cn (X. Xu), yan2000@whut.edu.cn (Y. Zhao), mlq518@whut.edu.cn (L. Mai).

https://doi.org/10.1016/j.ensm.2021.01.012
Received 12 November 2020; Received in revised form 22 December 2020; Accepted 12 January 2021
Available online 14 January 2021

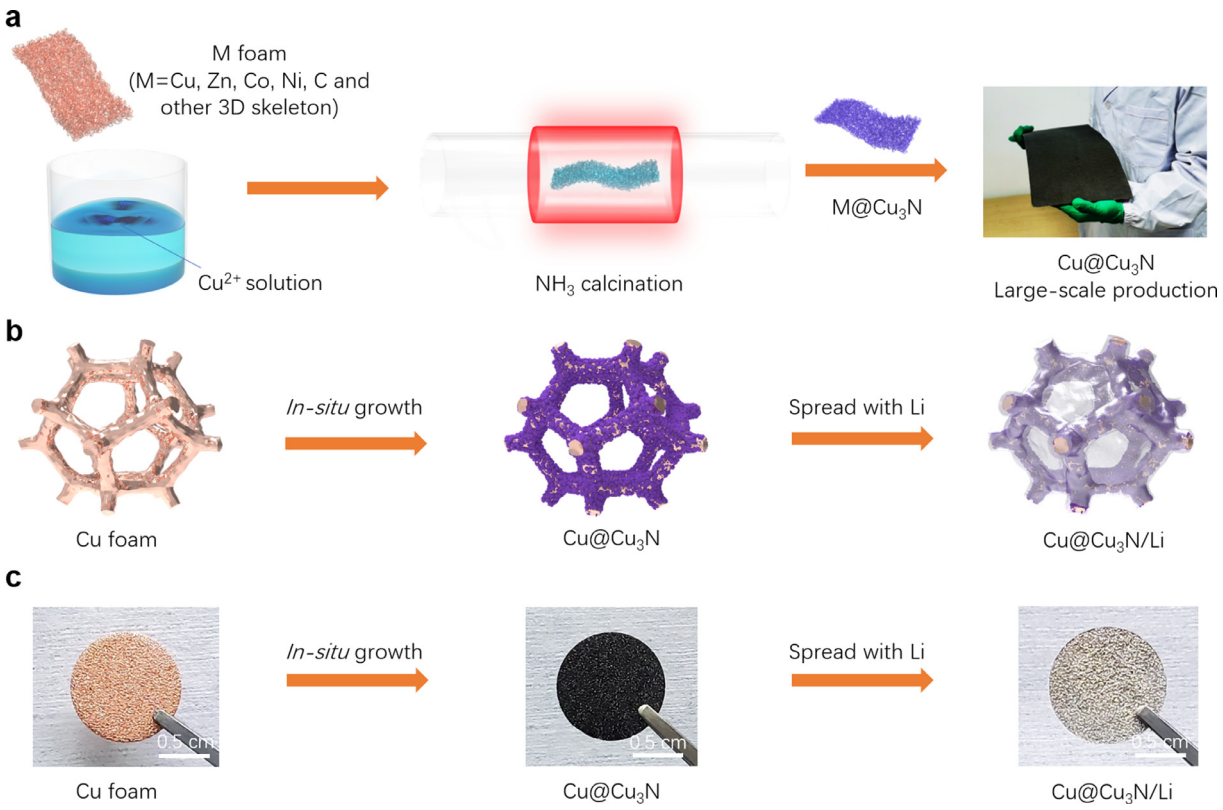

Fig. 1. Synthetic strategy. (a) Large–scale fabrication strategy, (b) Schematic of fabrication of Cu@Cu_3N/Li anode, (c) Optical images of Cu@Cu_3N/Li anode at different prepare stages.

the infiltration of molten Li into Cu@Cu_3N (Cu@Cu_3N/Li, Fig. S3), the Cu@Cu_3N realized a stable and dendrite–free Li plating/stripping under restricted conditions. Paired with $LiFePO_4$ (LFP) cathode, the full cell exhibited desirable cyclic stability with high active mass loading, limited Li resources and electrolyte, showing practical potential for the next generation of high–energy LMB.

2. Results and Discussion

The lithiophilicity testing process was investigated by *in–situ* optical observation of molten Li permeating into bare Cu foam (Cu), nitrogen–doped Cu foam (N–Cu), and Cu@Cu_3N (Fig. 2a–c). It shows that both Cu and N–Cu have a poor affinity with molten Li, even under deliberate pressure, the Li still cannot infuse into the substrates over 30 s (Videos S1 and S2). On the contrary, from the beginning of the contact between molten Li and Cu@Cu_3N, Li shows an obvious capillary infiltration phenomenon and quickly diffuses into the Cu@Cu_3N, and finally leaves a silver colored smooth substrate within 6 s (Video S3). This rapid Li diffusion behavior is due to the superior lithiophilicity of Cu_3N and the abundant Li nucleation sites (N–) along the Cu@Cu_3N framework. Furthermore, the successful preparation of Zn@Cu_3N, Co@Cu_3N, Ni@Cu_3N and C@Cu_3N and the corresponding excellent lithiophilicity have further extended the universality of this synthesis strategy in the protection of Li anode (Fig. S4 and S5).

To probe the Li metal electrodeposition behavior, an *in–situ* microscopic device was employed to visualize the real–time structure evolution of Li anodes (Fig. S6). At the initial deposition stage, there is no obvious different deposition behavior between Cu, N–Cu and Cu@Cu_3N within 3 min (Fig. 2d–f). With the extension of the deposition time, both Cu and N–Cu remain original surfaces without deposited Li, followed by presenting a large amount of prominent Li dendrites (Fig. S7). In contrast, the Cu@Cu_3N shows more homogeneous and stable Li deposition behavior during discharging, which is attributed to that the Cu_3N plays a significant role in promoting uniform Li nucleation and constructing high electronic/Li ion conductivity Li_3N ($Cu_3N + Li = Li_3N + Cu$) inorganic phase. [38] In order to confirm the conversion reaction of Cu_3N to Li_3N, the Cu@Cu_3N framework after the Li stripping was investigated by the X–ray diffraction (XRD) and etched X–ray photoelectron spectroscopy (XPS) techniques (Fig. S8 and S9). XRD patterns show that the typical crystalline phases of Cu and Cu_3N coexist in Cu@Cu_3N, meaning that the Cu@Cu_3N has a stable and compatible structure. Notably, the N–Cu shows the same crystalline phase of Cu, which presents that the N element is only adsorbed on the surface of Cu. Due to the high crystallinity of Cu and a thin layer of Cu_3N, the typical peaks of Li_3N crystal can not be found by XRD in the stripped sample. However, the characteristic peaks of Cu_3N also disappear from the XRD pattern, which indirectly proves that there was a certain chemical reaction occurring between the Cu_3N and Li. N1s XPS spectra further show that an obvious new peak appears at 399.2 eV of Cu@Cu_3N, which demonstrates that the Li_3N was formed by lithiation of Cu_3N.[43, 44]

Cycling stability of symmetric cells directly reveals the performance–enhancing effects of the Cu_3N coating. Specifically, the molten Li cannot be spread easily into the Cu and N–Cu skeletons due to their inferior wettability with Li as illustrated above, the fabrication details of Cu/Li and N–Cu/Li electrodes can be found in Supporting Information. The cycling performances of Cu@Cu_3N/Li, Cu/Li, and N–Cu/Li at a current density of 1 mA cm^{-2} with a capacity of 1 mAh cm^{-2} are shown in Fig. 3a. The symmetric cell with Cu@Cu_3N/Li displays a stable voltage response with only around 16 mV over 3,000 h (Fig. S10). In contrast, Cu/Li and N–Cu/Li show severe voltage hysteresis in the initial few cycles, and followed by steep increases and drops, leading to the cell short–circuit. It indicates that Cu@Cu_3N not only induces the uniform Li deposition, but also promotes highly reversible Li charge and discharge. In order to broaden the application of Cu@Cu_3N/Li in various electrolyte systems, the symmetric cells in conventional 1M $LiPF_6$ in ethylene carbonate/diethyl carbonate

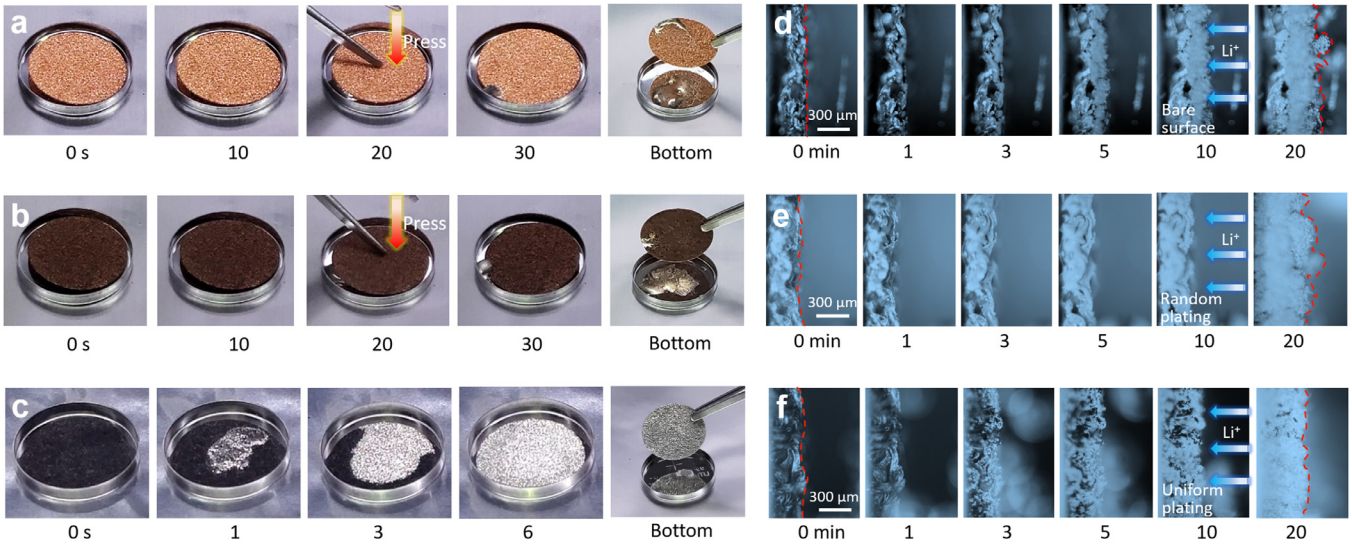

Fig. 2. *In–situ* microscope. (a–c) Optical images of spreading molten Li with Cu, N–Cu and Cu@Cu_3N, respectively, (d–f) *In–situ* microscopy images of Li electrochemical deposition behavior with Cu, N–Cu and Cu@Cu_3N, respectively.

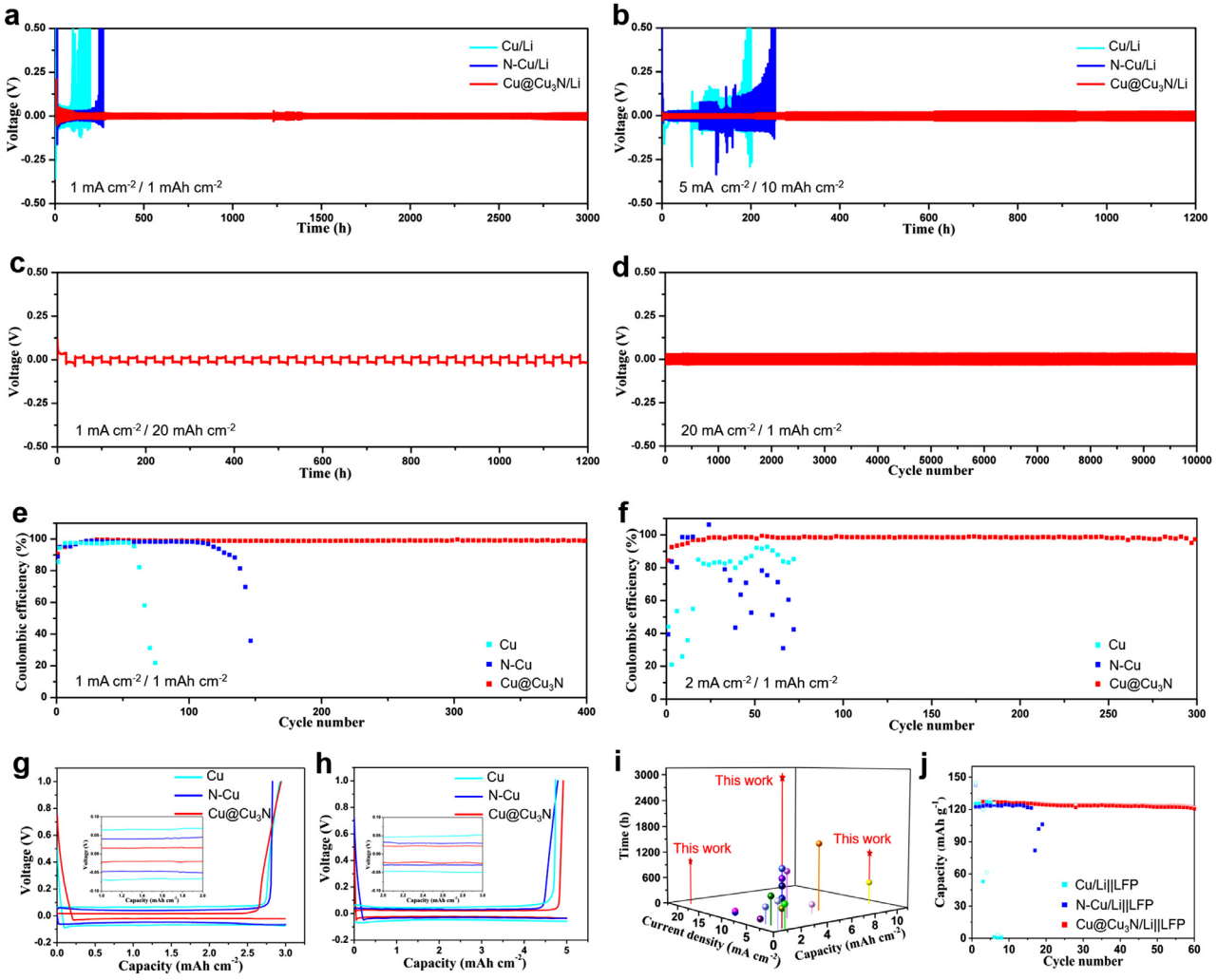

Fig. 3. Electrochemical performance. (a and b) Voltage profiles of Cu/Li, N–Cu/Li and Cu@Cu_3N/Li at 1 mA cm^{-2} for 1 mAh cm^{-2} and 5 mA cm^{-2} for 10 mAh cm^{-2}, respectively, (c and d) Cycling stability of Cu@Cu_3N/Li under deep and ultra–fast Li plating/stripping, respectively, (e and f) CE comparison of Cu, N–Cu and Cu@Cu_3N at 1 and 2 mA cm^{-2} for 1 mAh cm^{-2}, respectively, (g and h) Initial voltage profiles comparison of Cu, N–Cu, and Cu@Cu_3N at 1 mA cm^{-2} for 3 mAh cm^{-2} and 5 mAh cm^{-2}, respectively (inset is magnified voltage profiles), (i) Comparison of cycling stability in this work and a variety of previous reports on 3D Li current collector, (j) Cycling test of Cu@Cu_3N/Li||LFP under near real practical conditions at a current density of 1.6 mA cm^{-2}.

(1:1 by volume) carbonate electrolyte were investigated (Fig. S11). Obviously, the Cu@Cu_3N/Li shows the lowest voltage polarization with only around 18 mV over 300 h, while the Cu/Li shows an extremely voltage response and the N–Cu/Li presents a serious voltage polarization (40 mV). According to Sand's model prediction, [45] the Li dendrites is more likely to grow under more faster and deeper charge/discharge. However, the operation of LMB under moderate conditions would render its high energy advantage meaningless and restrict its application potential for high–power density systems (such as electric vehicles). [46,47] To illustrate this point, Fig. 3b shows the Cu@Cu_3N/Li, N–Cu/Li and Cu/Li cycling stability at 5 mA cm^{-2} for 10 mAh cm^{-2}. Obviously, Cu@Cu_3N/Li shows a more resilient cycle life and displays a negligible voltage polarization of around 24 mV compared to N–Cu/Li and Cu/Li, which benefits to meet the urgent requirements of high–energy/power LMB (Fig. S12). For a higher purpose of practical application, a deeper stripping/plating capacity of 20 mAh cm^{-2} under a constant current density (1 mA cm^{-2}) was evaluated here (Fig. 3c). The Cu@Cu_3N/Li shows a sable overpotential of 25 mV without any signs of failure over 1,200 h. Remarkably, the fast charge/discharge measurement of Cu@Cu_3N/Li exhibits an ultra–stable trend under a high current density of 20 mA cm^{-2} for 10,000 cycles (Fig. 3d, Fig. S13). Such quick and stable Li plating/stripping is mainly attributed to that the electrokinetic effect [42] accelerates the Li ions flux self–concentration and the highly ionic conductive Li_3N reduces the cell polarization.

In addition, the Coulombic efficiency (CE), determined by the ratio of Li stripping capacity to plating capacity, is another important indicator to measure the performance of Li anode. As illustrated in Fig. 3e and 3f, the Cu@Cu_3N shows a high reversible ratio of Li stripping capacity to plating capacity. When setting the capacity at 1 mAh cm^{-2}, CE of 99.2% and 98.3% were delivered after 400 cycles at 1 mA cm^{-2} and after 300 cycles at 2 mA cm^{-2}, respectively. However, the CE of Cu and N–Cu sharply decreases to < 30% only in short cycles, suggesting that uncontrollable Li plating/stripping occurred inside the cells. Even under deep charge and discharge, CE of 98.5% and 98.4% and stable charge–discharge profiles were obtained at 1 mA cm^{-2} for 3 mAh cm^{-2} and 5 mAh cm^{-2}, respectively (Fig. S14). Moreover, the corresponding voltage gaps of 42 and 46 mV at 1 mA cm^{-2} for 3 and 5 mAh cm^{-2} were realized of Cu@Cu_3N, much lower than those of Cu (133 and 96 mV) and N–Cu (98 and 60 mV) (Fig. 3g and 3h). Compare with other latest reported current collectors (Table S1), Cu@Cu_3N shows obvious advantages in cycle life and faster charging and discharging ability (Fig. 3i). These findings demonstrate that the Li is seeded due to the presence of Cu_3N with highly reversible abundant Li nucleation sites for whole Cu@Cu_3N, which boosts bright development of LMB for high–energy electric vehicles application.

The electrochemical performances of the full cells paired Cu@Cu_3N/Li, N–Cu/Li and Cu/Li anodes with sulfur (Cu@Cu_3N/Li||S, N–Cu/Li||S and Cu/Li||S), $LiNi_{0.8}Mn_{0.1}Co_{0.1}O_2$ (Cu@Cu_3N/Li||NMC811, N–Cu/Li||NMC811 and Cu/Li||NMC811) and LFP (Cu@Cu_3N/Li||LFP, N–Cu/Li||LFP and Cu/Li||LFP) cathodes were evaluated. In the unstable Li||S and Li||NMC811 (cut–off voltage is 4.5 V) systems, the Cu@Cu_3N/Li||S and Cu@Cu_3N/Li||NMC811 full cells show enhanced cycling stability compared to those of Cu/Li||S, N–Cu/Li||S and Cu/Li||NMC811, N–Cu/Li||NMC811 full cells, respectively (Fig. S15). This finding indicates that the improvement of Li anode is an effective approach to improve the lifespan of LMB. In the stable LFP system, the batteries became invalid directly only after 200 cycles with Cu/Li and N–Cu/Li anodes, which is mainly attributed to the failure of the anode side. On the contrary, Cu@Cu_3N/Li||LFP shows a persistent cycling ability and desirable rate performance (Fig. S16), especially under 3.0 C rate, a capacity retention of 86% was obtained after 3,000 cycles, implying the Cu_3N is the optimal choice to solve various unstable issues of Li anode and improve the LMB life of great significance. Furthermore, the electrochemical impedance spectroscopy (EIS) results show that the Cu@Cu_3N/Li||LFP has a lower charge transfer resistance (80.18 Ω) than those of Cu/Li||LFP (392.25 Ω) and N–Cu/Li||LFP (126.39 Ω), which is owing to the fast and homogeneous Li ions supplement from the Cu@Cu_3N/Li anode (Fig. S17). The higher diffusion coefficient D_{Li^+} of the Cu@Cu_3N/Li||LFP shows that the Cu@Cu_3N/Li promotes the Li ions transportation between the cathode and anode, resulting in stable and high reversible electrochemical reaction inside the battery (Table S2).

Ultimately, however, to achieve the high–energy LMB, the active materials loading, Li anode areal capacity utilization, negative/positive (N/P) electrode capacity ratio, and the electrolyte/active mass loading (E/A) ratio are critical factors. [48–50] Firstly, a high cathode capacity requires a large amount of Li plate/strip in each cycle, thus, constructing a stable Li anode is essential. Secondly, in normal cycles, the electrolyte would be fast consumed in the first few cycles due to the formation of SEI, so stabilizing the circulation in such a barren electrolyte is such a huge challenge. Here, the Cu@Cu_3N/Li||LFP and control full cells with LFP mass loading of 19.1 mg cm^{-2} (3.25 mAh cm^{-2}), N/P of 3.2 (Li capacity is limited to 10.24 mAh cm^{-2}) and the E/A of 2.3 were fabricated. The cycling test shows that the Cu/Li||LFP and N–Cu/Li||LFP full cells are rapidly depleted in a short term, while the Cu@Cu_3N/Li||LFP presents a stable cycle life almost with no capacity fading at a current density of 1.6 mA cm^{-2} (Fig. 3j). The corresponding CE maintained at as high as 99.3%, indicating the excellent electrodes structure stability and electrochemical reversibility of both cathode and anode. The charge/discharge profiles of Cu@Cu_3N/Li||LFP show no obvious change during cycling, and a lower overpotential (around 0.23V) indicates that the Li/electrolyte interface is highly stable (Fig. S18). Furthermore, an excellent rate performance was achieved under such demanding test conditions, and the cell did not breakdown even at 5.0 C rate with a reversible capacity up to 60 mAh g^{-1}. With the decrease of the current density, the capacity is also gradually recovered, which further indicates the good stability and compatibility of the whole Cu@Cu_3N/Li||LFP full cell. All these findings reveal that the Cu@Cu_3N/Li anode can match well with different cathodes and display promising potential industrial availability for high–energy LMB.

To further confirm the stable structure and Li dendrite–free feature of Cu@Cu_3N/Li anode, the electrodes after different Li plating/stripping cycles were investigated by scanning electron microscope (SEM) measurement. It is clearly observed that Cu/Li (Fig. 4a–d) and N–Cu/Li (Fig. 4e–h) electrodes present severe degradation within short cycles (10 th), and the dense structure of the whole electrode appears to be highly porous, indicating a lot of "dead Li" were produced and SEI was broken. In addition, the thickness of the Cu/Li and N–Cu/Li electrodes expanded from initial 300 μm to 532 μm (77% increase) and 493 μm (64% increase) after 100 cycles, respectively, and a large number of Li dendrites and "dead Li" generated on the electrode surface (Fig. 4d and 4h, and Fig. S19). As consequences of the lithiophobic materials, the severely increased thickness of Cu/Li and N–Cu/Li electrodes are mainly caused by the following issues: (1) low CE, (2) internal Li stripping and preferred surface deposition, and (3) the electrolyte penetration of the porous electrode, resulting in consumption of extra Li and more side reactions. On the contrary, the integrity of the Cu@Cu_3N/Li anode structure has no obvious change throughout the 100 cycles (Fig. 4i–k). After completing 100 cycles, the thickness only increased to 318 μm (6% increase) and a small amount of Li pieces were observed on the surface (Fig. 4l), which proves the well–regulated 3D structure of lithiophilic Cu@Cu_3N effectively promotes the uniform Li plating/stripping and maintains the anode safety and stability.

Fig. 5a shows the mechanism of Li deposition on Cu or N–Cu substrates. Due to their poor–lithiophilicity, neither the molten Li nor the Li ions enable bounded to their skeleton, and Li is prefer rigidly depositing on the surface after long–time infusing. The lower Li ions distributions near the surface of current collector than that at other parts will lead selective deposition of Li ions, causing the growth of dendrite during repeated Li plating/stripping. Moreover, the severe deformation of the electrode leads to the continuous consumption of electrolyte and

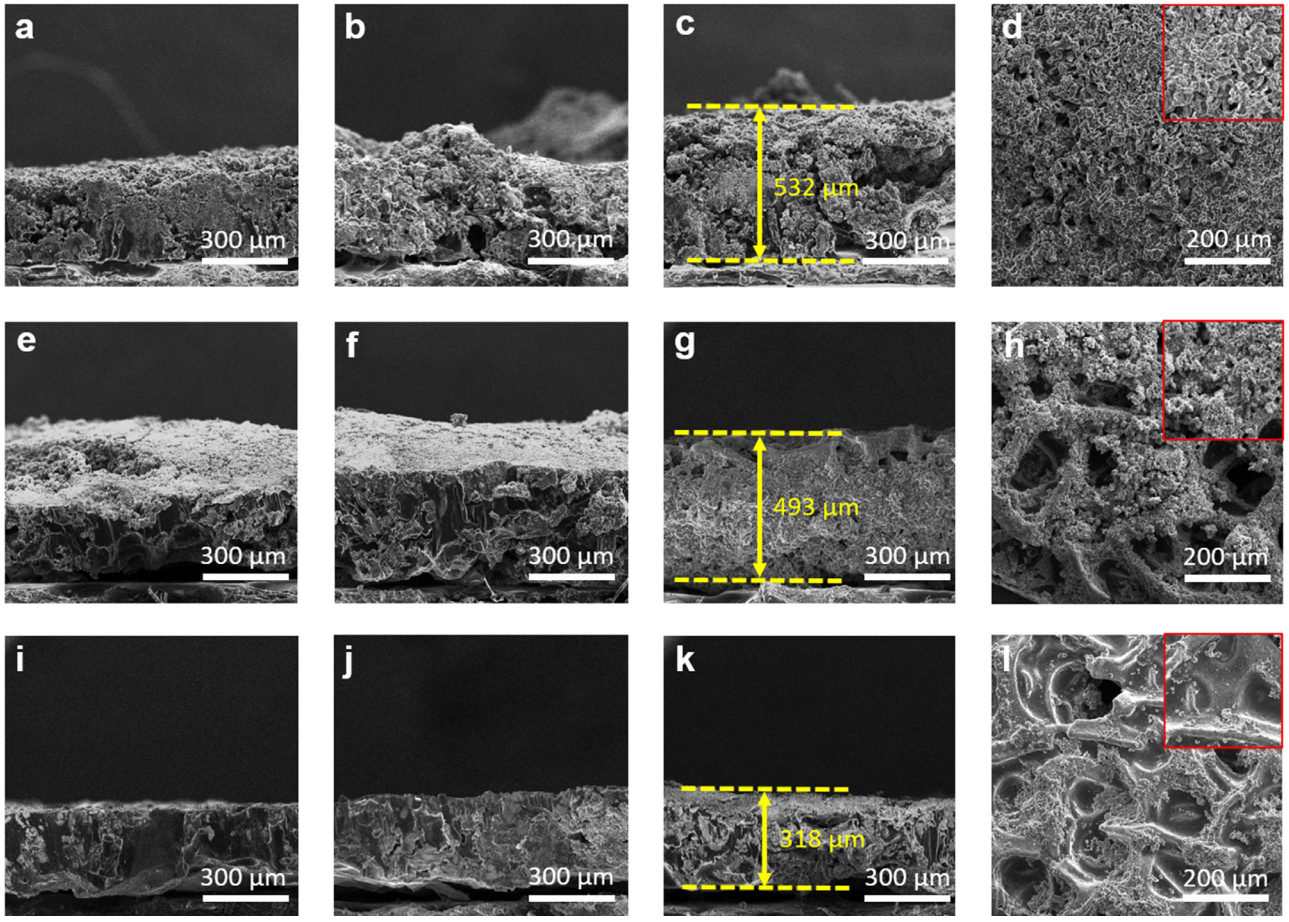

Fig. 4. Morphology evolution after cycling. (a–c), (e–g) and (i–k) Side SEM images of Cu/Li, N–Cu/Li and Cu@Cu_3N/Li end with 10, 50 and 100 cycles at 1 mA cm^{-2} for 1 mAh cm^{-2}, respectively, (d, h and l) Top view of (c), (g) and (k), respectively, and each inset is the corresponding magnified image.

uncontrollable SEI formation on the refresh Li anode surface. On the contrary, the Li dendrites and SEI is significantly restricted due to the self–concentration of Li ions at the anode/electrolyte interface, resulting in uniform Li ions flux distribution and homogenous Li plating/stripping (Fig. 5b).

As the advantages of Cu@Cu_3N were presented above, first principles calculations are performed here for developing a thorough understanding of the lithiophilic nature of Cu_3N. Fig. S20 shows the surface energy of Cu and Cu_3N. According to its definition, the material grows preferentially along the crystal surface with low surface energy. Therefore, Cu (111) and Cu_3N (100) with the lowest surface energies are selected for the study of Li binding. The binding energies (Fig. 5c and Fig. S21) of Li to Cu (111) and Cu_3N (100) are −0.79 eV and −1.12 eV, respectively, showing that Cu_3N has a stronger affinity to Li. In addition, Li has a shorter bond length with Cu_3N (1.88 Å) than Cu (2.28 Å), indicating that Li is more willing to get close to Cu_3N. Bader charge analysis also proves the stronger bonding of Li to Cu_3N than Cu by a more positive charge of the adsorbed Li (+0.88 and +0.66, respectively). The differential charges (Fig. 5d) also display that the weak physical interaction (Li–Cu) is mainly between Li and Cu, while the stronger ionic bond (Li–N) exists in in Li_3N resulting from the reaction of Li and Cu_3N.[51] The migration paths of Li in Cu and Cu_3N intuitively show that Cu_3N has broader one–dimensional transport channels (Fig. S22). The corresponding migration energy barrier curves show that Li has a much lower migration energy barrier in Cu_3N (Fig. 5e), indicating the Li ions on the surface of Cu_3N can further diffuse and redistribute. Finally, a "radar" model was proposed here for safe Li metal alternatives, which should meet the following 6 characteristics: lithiophilicity, conductivity, stability, specific area, flexibility, and scalability (Fig. 5f).

As a whole, the mechanism of uniform Li ions transfer can be revealed in the following three aspects: (1) Due to the strong affinity between Li and Cu_3N, Li ions will self–concentration on the electrode surface, which means that after Li depositing on the electrode surface, the Li ions in the electrolyte will replenish immediately, leading to high Li ion concentration at the electrode/electrolyte interface. (2) Low migration energy barrier accelerates fast adsorbed Li ions detach along the entire electrode surface, resulting in dendrite–free Li metal anode. (3) Because of the synergistic effect of this compatible structure, the uniform Li ions distribution and minimized polarization are achieved in long lived anode.

3. Conclusion

In summary, this ultra–lithiophilic Cu@Cu_3N has been successfully prepared via a facile and novel scalable method. The compatible structure can not only effectively reduce the local current density due to its large surface area, but also provide enough space to minimize the theoretical infinite volume expansion of Li. Furthermore, the electrokinetic effect significantly promotes the Li ions transport, which is induced by the enhanced electrokinetic surface conduction owing to the lithiophilic Cu_3N. Compared with Cu and N–Cu, an enhanced lithiophilicity and homogeneous Li deposition for the Cu@Cu_3N has been demonstrated by *in–situ* microscopic measurement. Under near practical conditions, Cu@Cu_3N exhibited surprising electrochemical performance in both half– and full cells. The first principles calculations give a deep understanding of the lithiophilicity nature of Cu_3N, offering theoretical support to our design concept for current collector, which provides a promising prospect to high–energy and long–life LMB.

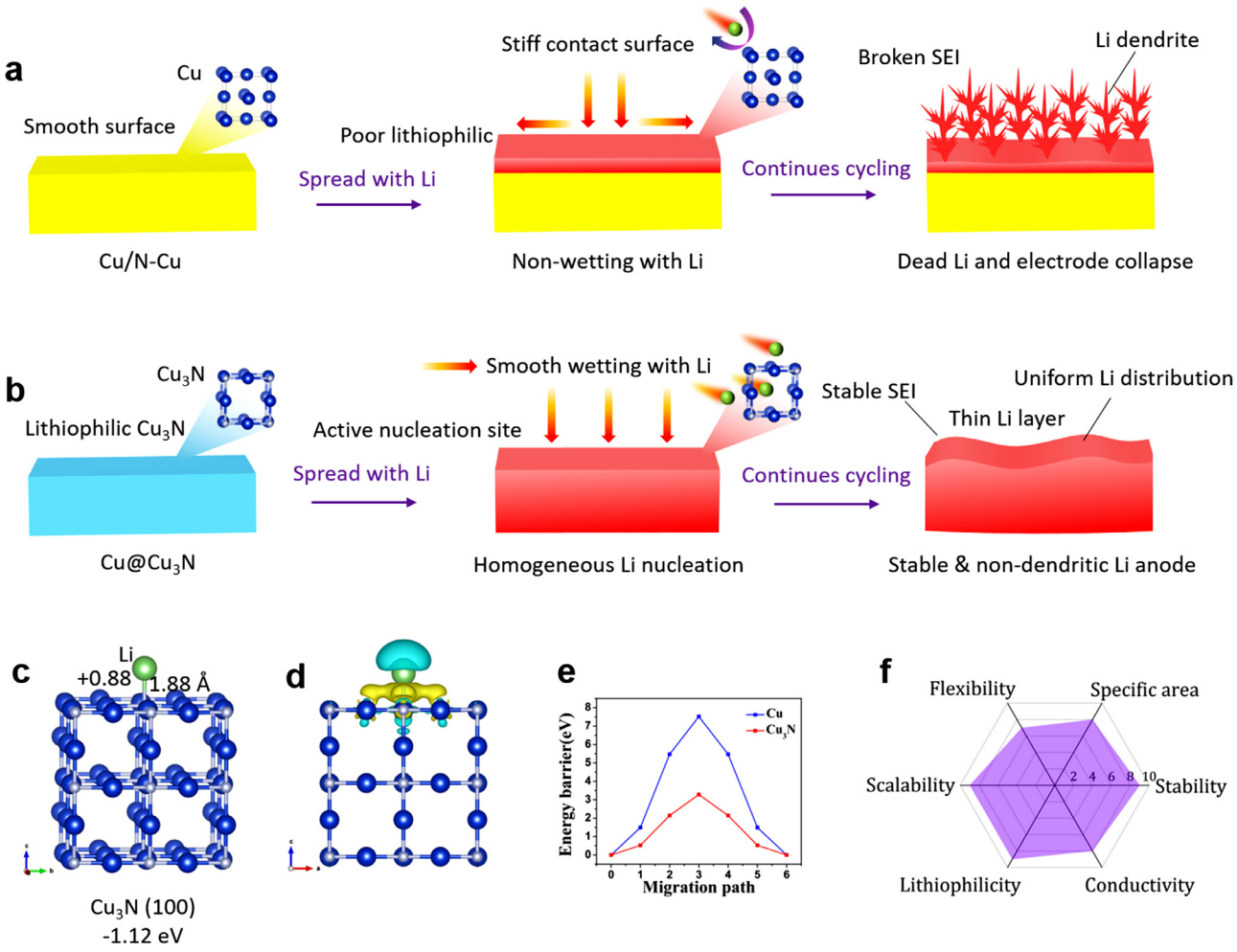

Fig. 5. Lithiophilicity mechanism and first principles calculations. (a and b) Mechanism schematic of Li deposition on Cu, N–Cu and Cu@Cu_3N, (c) Structure optimization of Li to Cu_3N, (d) Differential charge of (a), (e) Migration path of Li in Cu_3N and corresponding migration barriers, (f) Radar signature of Cu@Cu_3N.

Credit author statement

L.Q. Mai and X. Xu conceived and supervised this project. Z.H. Li and Q. He designed the experiments, analyzed the results and wrote the manuscript. Z.H. Li, Y. Li, C. Zhou, Z.H. Liu, and X.F. Hong performed the experiments and analyzed the results. Z.H. Li, Y. Zhao and Q. He performed the DFT computations and theoretical analyses. All the authors participated in the revision and discussion of the manuscript.

Declaration of Competing Interest

The authors declare they have no known competing financial interests or personal relationships that could have appeared to influence the work reported in this paper.

Acknowledgements

This work was supported by the National Key Research and Development Program of China (2020YFA0715000, 2016YFA0202603), the National Natural Science Foundation of China (51832004, 51521001), Foshan Xianhu Laboratory of the Advanced Energy Science and Technology Guangdong Laboratory (XHT2020-003), the Program of Introducing Talents of Discipline to Universities (B17034), the Yellow Crane Talent (Science & Technology) Program of Wuhan City, the National Natural Science Foundation of China and the Fundamental Research Funds for the Central Universities (WUT: 2019III174, 2020III023, 2020III050).

Supplementary materials

Supplementary material associated with this article can be found, in the online version, at doi:10.1016/j.ensm.2021.01.012.

References

[1] D. Lin, Y. Liu, Y. Cui, Reviving the lithium metal anode for high–energy batteries, Nat. Nanotechnol. 12 (2017) 194–206.
[2] P. Albertus, et al., Status and challenges in enabling the lithium metal electrode for high–energy and low–cost rechargeable batteries, Nat. Energy 3 (2017) 16–21.
[3] J. Chen, et al., Electrolyte design for LiF–rich solid–electrolyte interfaces to enable high–performance microsized alloy anodes for batteries, Nat. Energy 5 (2020) 386–397.
[4] T. Chen, et al., Dendrite–Free and Stable Lithium Metal Anodes Enabled by an Antimony–Based Lithiophilic Interphase, Chem. Mater. 31 (2019) 7565–7573.
[5] C. Niu, et al., Self–smoothing anode for achieving high–energy lithium metal batteries under realistic conditions, Nat. Nanotechnol. 14 (2019) 594–601.
[6] X. Liang, et al., A facile surface chemistry route to a stabilized lithium metal anode, Nat. Energy 2 (2017) 17119.
[7] S. Chen, F. Dai, M. Cai, Opportunities and Challenges of High–Energy Lithium Metal Batteries for Electric Vehicle Applications, ACS Energy Lett 5 (2020) 3140–3151.
[8] D.H. Liu, et al., Developing high safety Li–metal anodes for future high–energy Li–metal batteries: strategies and perspectives, Chem. Soc. Rev. 49 (2020) 5407–5445.
[9] Z. Luo, et al., Dendrite–free lithium metal anode with lithiophilic interphase from hierarchical frameworks by tuned nucleation, Energy Storage Mater 27 (2020) 124–132.
[10] Y. Gao, et al., Polymer–inorganic solid–electrolyte interphase for stable lithium metal batteries under lean electrolyte conditions, Nat. Mater. 18 (2019) 384–389.
[11] R. Xu, et al., Artificial Interphases for Highly Stable Lithium Metal Anode, Matter 1 (2019) 317–344.

[12] Z. Cao, B. Li, S. Yang, Dendrite–Free Lithium Anodes with Ultra–Deep Stripping and Plating Properties Based on Vertically Oriented Lithium–Copper–Lithium Arrays, Adv. Mater. 31 (2019) e1901310.
[13] H. Yuan, et al., An ultrastable lithium metal anode enabled by designed metal fluoride spansules, Sci. Adv. 6 (2020) eaaz3112.
[14] S.–Y. Li, et al., A facile strategy to reconcile 3D anodes and ceramic electrolytes for stable solid–state Li metal batteries, Energy Storage Mater 32 (2020) 458–464.
[15] Z. Luo, et al., Interfacial challenges towards stable Li metal anode, Nano Energy 79 (2021) 105507.
[16] M. Wan, et al., Mechanical rolling formation of interpenetrated lithium metal/lithium tin alloy foil for ultrahigh–rate battery anode, Nat. Commun. 11 (2020) 829.
[17] L. Chen, et al., High–Energy Li Metal Battery with Lithiated Host, Joule 3 (2019) 732–744.
[18] H. Duan, et al., Uniform Nucleation of Lithium in 3D Current Collectors via Bromide Intermediates for Stable Cycling Lithium Metal Batteries, J. Am. Chem. Soc. 140 (2018) 18051–18057.
[19] Y.–G. Lee, et al., High–energy long–cycling all–solid–state lithium metal batteries enabled by silver–carbon composite anodes, Nat. Energy 5 (2020) 299–308.
[20] S.S. Chi, et al., Lithiophilic Zn Sites in Porous CuZn Alloy Induced Uniform Li Nucleation and Dendrite–free Li Metal Deposition, Nano Lett 20 (2020) 2724–2732.
[21] W. Zhang, et al., A "cation–anion regulation" synergistic anode host for dendrite–free lithium metal batteries, Sci. Adv. 4 (2018) eaar4410.
[22] G. Huang, et al., Lithiophilic 3D Nanoporous Nitrogen–Doped Graphene for Dendrite–Free and Ultrahigh–Rate Lithium–Metal Anodes, Adv. Mater. 31 (2019) 1805334.
[23] L. Luo, et al., A 3D Lithiophilic Mo_2N–Modified Carbon Nanofiber Architecture for Dendrite–Free Lithium–Metal Anodes in a Full Cell, Adv. Mater. 31 (2019) 1904537.
[24] X. Zhang, et al., MXene Aerogel Scaffolds for High–Rate Lithium Metal Anodes, Angew. Chem. 57 (2018) 15028–15033.
[25] Z. Liang, et al., Composite lithium metal anode by melt infusion of lithium into a 3D conducting scaffold with lithiophilic coating, Proc. Natl. Acad. Sci. USA 113 (2016) 2862–2867.
[26] M.C. Stan, et al., Sputter coating of lithium metal electrodes with lithiophilic metals for homogeneous and reversible lithium electrodeposition and electrodissolution, Mater. Today, 2020.
[27] Y. Gu, et al., Lithiophilic Faceted Cu(100) Surfaces: High Utilization of Host Surface and Cavities for Lithium Metal Anodes, Angew. Chem. 58 (2019) 3092–3096.
[28] P. Shi, et al., Lithiophilic LiC_6 Layers on Carbon Hosts Enabling Stable Li Metal Anode in Working Batteries, Adv. Mater. 31 (2019) 1807131.
[29] X. Chen, et al., Lithiophilicity chemistry of heteroatom–doped carbon to guide uniform lithium nucleation in lithium metal anodes, Sci. Adv. 5 (2019) eaau7728.
[30] R. Zhang, et al., Coralloid Carbon Fiber–Based Composite Lithium Anode for Robust Lithium Metal Batteries, Joule 2 (2018) 764–777.
[31] K. Li, et al., A 3D and Stable Lithium Anode for High–Performance Lithium–Iodine Batteries, Adv. Mater. 31 (2019) 1902399.
[32] T. Zhang, et al., Stable Lithium Metal Anode Enabled by a Lithiophilic and Electron/Ion Conductive Framework, ACS Nano 14 (2020) 5618–5627.
[33] G.Y. Jiang, et al., MOF–derived porous Co_3O_4–NC nanoflake arrays on carbon fiber cloth as stable hosts for dendrite–free Li metal anodes, Energy Storage Mater 23 (2019) 181–189.
[34] S.H. Wang, et al., Tuning wettability of molten lithium via a chemical strategy for lithium metal anodes, Nat. Commun. 10 (2019) 4930.
[35] D. Zhang, et al., Lithiophilic 3D Porous CuZn Current Collector for Stable Lithium Metal Batteries, ACS Energy Lett 5 (2019) 180–186.
[36] Z. Luo, et al., Dendrite–free lithium metal anode with lithiophilic interphase from hierarchical frameworks by tuned nucleation, Energy Storage Mater 27 (2020) 124–132.
[37] K. Park, J.B. Goodenough, Dendrite–Suppressed Lithium Plating from a Liquid Electrolyte via Wetting of Li_3N, Adv. Energy Mater. 7 (2017) 1700732.
[38] Y. Liu, et al., Solubility–mediated sustained release enabling nitrate additive in carbonate electrolytes for stable lithium metal anode, Nat. Commun. 9 (2018) 3656.
[39] Y. Liu, et al., An Artificial Solid Electrolyte Interphase with High Li–Ion Conductivity, Mechanical Strength, and Flexibility for Stable Lithium Metal Anodes, Adv. Mater. 29 (2017) 1605531.
[40] Q. Li, et al., Homogeneous Interface Conductivity for Lithium Dendrite–Free Anode, ACS Energy Lett 3 (2018) 2259–2266.
[41] D. Lee, et al., Copper Nitride Nanowires Printed Li with Stable Cycling for Li Metal Batteries in Carbonate Electrolytes, Adv. Mater. 32 (2020) 1905573.
[42] Q. Shi, et al., High–capacity rechargeable batteries based on deeply cyclable lithium metal anodes, Proc. Natl. Acad. Sci. USA 115 (2018) 5676–5680.
[43] G. Li, et al., Stable metal battery anodes enabled by polyethylenimine sponge hosts by way of electrokinetic effects, Nat. Energy 3 (2018) 1076–1083.
[44] K.S. Yook, et al., Air stable and low temperature evaporable Li_3N as a n type dopant in organic light–emitting diodes, Synth. Met. 159 (2009) 1664–1666.
[45] M.S. Kim, et al., Langmuir–Blodgett artificial solid–electrolyte interphases for practical lithium metal batteries, Nat. Energy 3 (2018) 889–898.
[46] C. Brissot, et al., Concentration measurements in lithium/polymer–electrolyte/lithium cells during cycling, J. Power Sources 94 (2001) 212–218.
[47] J.–Y. Hwang, et al., Customizing a Li–metal battery that survives practical operating conditions for electric vehicle applications, Energy Environ. Sci. 12 (2019) 2174–2184.
[48] Z. Jiang, et al., Facile Generation of Polymer–Alloy Hybrid Layers for Dendrite–Free Lithium–Metal Anodes with Improved Moisture Stability, Angew. Chem. 58 (2019) 11374–11378.
[49] X.Q. Zhang, et al., A Sustainable Solid Electrolyte Interphase for High–Energy–Density Lithium Metal Batteries Under Practical Conditions, Angew. Chem. 59 (2020) 3252–3257.
[50] J. Xie, et al., Incorporating Flexibility into Stiffness: Self–Grown Carbon Nanotubes in Melamine Sponges Enable A Lithium–Metal–Anode Capacity of 15 mA h cm^{-2} Cyclable at 15 mA cm^{-2}, Adv. Mater. 31 (2019) 1805654.
[51] H. Park, et al., Lithiophilic surface treatment of metal– and metallic compound–basedframeworks by gas nitriding for lithium metal batteries, J. Power Sources 477 (2020) 228776.